*energies*

MDPI

*Article*

# Two-Stage Robust Optimization Model for Flexible Response of Micro-Energy Grid Clusters to Host Utility Grid

**Hongkai Zhang [1], Outing Zhang [2,*], Peng Li [1], Xianyu Yue [1] and Zhongfu Tan [2]**

[1] Economic Research Institute, State Grid Henan Electric Power Company, Zhengzhou 450052, China
[2] School of Economics and Management, North China Electric Power University, Beijing 102206, China
* Correspondence: 120232206091@ncepu.edu.cn

**Abstract:** As a decentralized energy management paradigm, micro-energy grid (MEG) clusters enable synergistic operation of heterogeneous distributed energy assets, particularly through multi-energy vector coupling mechanisms that enhance distributed energy resource (DER) utilization efficiency in next-generation power networks. While individual MEGs demonstrate limited capability in responding to upper-grid demands using surplus energy after fulfilling local supply/demand balance, coordinated cluster operation significantly enhances system-wide flexibility. This paper proposes a two-stage robust optimization model that systematically addresses both the synergistic complementarity of multi-MEG systems and renewable energy uncertainty. First, the basic operation structure of MEG, including distributed generation, cogeneration units, and other devices, is established, and the operation mode of the MEG cluster responding to host utility grid flexibly is proposed. Then, aiming to reduce operation expenses, an optimal self-scheduling plan is generated by establishing a MEG scheduling optimization model; on this basis, the flexibility response capability of the MEG is measured. Finally, to tackle the uncertainty issue of wind and photovoltaic power generation, the two-stage robust theory is employed, and the scheduling optimization model of MEG cluster flexibility response to the host utility grid is constructed. A southern MEG cluster is chosen for simulation to test the model and method's effectiveness. Results indicate that the MEG cluster's flexible response mechanism can utilize individual MEGs' excess power generation to meet the host utility grid's dispatching needs, thereby significantly lowering the host utility grid's dispatching costs.

**Keywords:** micro-energy grid cluster; flexible response; two-stage robust optimization; host utility grid

check for updates

Academic Editor: Michael Negnevitsky

Received: 8 May 2025
Revised: 26 May 2025
Accepted: 5 June 2025
Published: 7 June 2025

**Citation:** Zhang, H.; Zhang, O.; Li, P.; Yue, X.; Tan, Z. Two-Stage Robust Optimization Model for Flexible Response of Micro-Energy Grid Clusters to Host Utility Grid. *Energies* **2025**, *18*, 3030. https://doi.org/10.3390/en18123030

**Copyright:** © 2025 by the authors. Licensee MDPI, Basel, Switzerland. This article is an open access article distributed under the terms and conditions of the Creative Commons Attribution (CC BY) license (https://creativecommons.org/licenses/by/4.0/).

## 1. Introduction

Driven by the twin policy/technoeconomic imperatives of achieving carbon neutrality and accelerating grid decentralization dynamics, distribution network integration levels of distributed energy resources (DERs) exhibit sustained exponential growth patterns. As a paradigm of emerging multi-energy coupled systems, micro-energy grids (MEGs) facilitate energy cascade utilization and complementary coordination through electricity/gas/heat multi-energy flow coupling and conversion facilities [1]. This architecture effectively enhances renewable energy accommodation capacity at the distribution network level [2,3], positioning MEGs as critical infrastructure components in future low-carbon power systems. Upon achieving internal supply/demand balance, MEGs can operate as aggregated flexibility resource units to promptly respond to the scheduling needs of the host utility grid and provide flexible response output.

Contemporary investigations into MEGs predominantly center on operational architectures and dispatch optimization. Reference [4] conducts multi-energy coupling analysis and coordinated utilization of electricity, thermal, and natural gas systems within MEGs to satisfy diversified end-user load demands. Reference [5] integrates electric vehicles with mobile energy storage characteristics and demand response (DR) into MEG energy management, proposing a coordinated dispatch framework that effectively reduces operational costs and carbon emissions. Reference [6] designs a multi-objective dispatch strategy considering hybrid energy storage system configuration, achieving balanced trade-offs between economic efficiency and environmental sustainability. Although these studies demonstrate improved local efficiency, they inadequately address the systematic quantification of MEG clusters' flexibility potential for upper-grid interactions. While references [7,8] proposed real-time coordination mechanisms for multi-MEG systems, they lacked formalized metrics to convert DER flexibility into grid-dispatchable services, such as surplus generation thresholds or demand response depth. This oversight limits the practical integration of MEG clusters into electricity markets, where precise bidding parameters and cost-optimal response strategies are essential [9,10].

A second limitation lies in the simplistic treatment of renewable energy uncertainty. Reference [11] develops a stochastic optimization method addressing source/load uncertainty and their correlation coefficients, significantly enhancing operational flexibility. Reference [12] employs interval optimization theory to formulate optimal dispatch strategies by modeling load uncertainty as bounded intervals. Conventional approaches often rely on static probability distributions or rigid uncertainty bounds, failing to account for extreme scenarios like abrupt solar curtailments or spatially correlated wind forecast errors. Reference [13] applies stochastic programming with the Vine-Copula and TimeGAN methods for scenario generation of source/load uncertainties, enhancing prediction accuracy. Reference [14] proposes a bi-level cyber–physical coordination framework with multi-temporal resolution to strengthen system resilience against uncertainty risks. Although the above approaches have enhanced uncertainty modeling, they neglect the synergistic risk-pooling effects inherent to multi-MEG clusters. Consequently, these models produce overly conservative or economically suboptimal schedules, undermining their applicability in high-renewable penetration grids.

Furthermore, prevailing MEG studies exhibit a disconnect from evolving policy and market realities. Reference [15] establishes a bi-level optimization model that balances user satisfaction with renewable energy consumption preferences, effectively mitigating peak/valley load disparities. Reference [16] builds a two-tier framework for day-ahead and real-time energy trading of multi-MEG clusters, demonstrating enhanced system flexibility and reduced operational costs through inter-MEG collaboration. Reference [17] proposes a bi-level adaptive robust decision-making framework for co-optimizing techno-economic performance and grid-supportive functionality in multi-energy industrial microgrids. Reference [18] presents a scheduling model of island MEG that integrates biomass conversion systems, seawater desalination, and hydrogen production from electricity. While frameworks like bi-level energy trading and microgrid optimization advance technical coordination, they overlook critical economic drivers such as carbon pricing mechanisms and ancillary service market protocols. This omission restricts their relevance to jurisdictions actively implementing decarbonization mandates, where DER aggregation must align with regulatory incentives and grid-code compliance.

In conclusion, to fully exploit the flexibility response potential of MEGs toward host utility grids, this study proposes a two-stage robust optimization model that integrates multi-MEG synergistic complementarity and addresses renewable energy uncertainty. Firstly, an MEG structure including combined heat and power (CHP) units and DERs is

established, and the operation mode of the MEG cluster flexibly responding to the host utility grid is proposed. Subsequently, an MEG scheduling optimization model is constructed with the objective of reducing operational costs, and its flexible response capacity is evaluated. Finally, the two-stage robust theory is applied to address the uncertainty in wind and photovoltaic (PV) generation. On this basis, a two-stage robust optimization model for the flexibility response of an MEG cluster to the higher-level power grid is built, and a case study is designed to demonstrate the effectiveness and applicability of the model presented in this paper.

## 2. Flexibility Response Scheme of Micro-Energy Grid Clusters

### *2.1. Basic Operating Structure*

The fundamental components within an MEG comprise CHP units, DERs, energy storage devices, and end-users. Among these, CHP units serve as the primary energy supply infrastructure, delivering stable electrical and thermal energy to users. Distributed generation systems, including decentralized wind turbines (WTs) and PV installations, offer substantial generation potential while exhibiting significant output uncertainty. Energy storage systems perform critical peak-shaving and valley-filling functions for net internal load management, leveraging their rapid charge/discharge characteristics to mitigate power fluctuations from distributed generation. End-users demonstrate demand elasticity, which enables optimized energy consumption behaviors through incentive signals provided by MEG operators. The fundamental structure of the MEG is depicted in Figure 1.

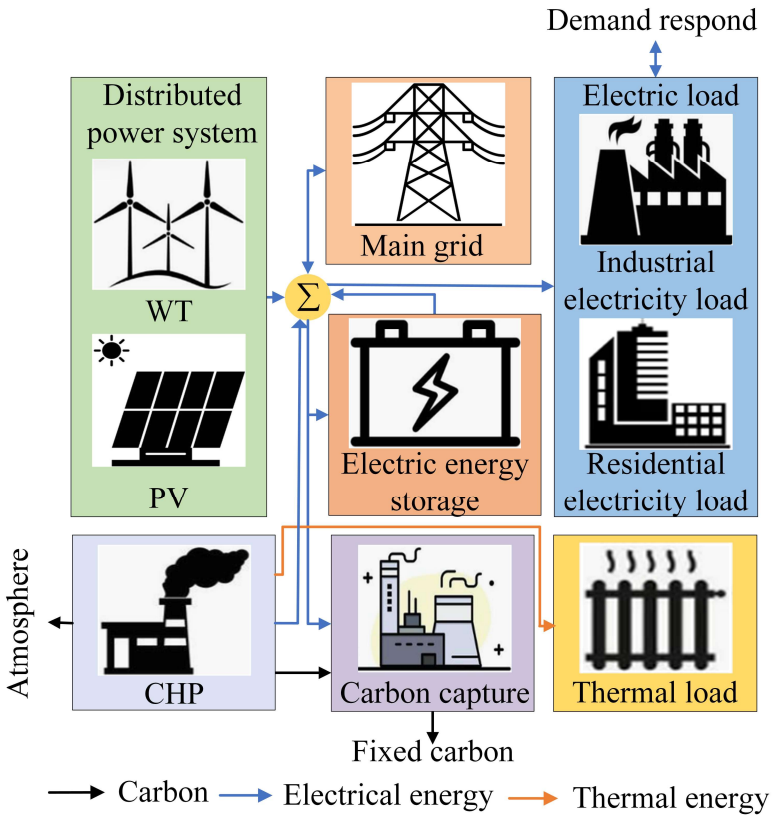



**Figure 1.** Basic structure diagram of MEG.

### *2.2. Each-Unit Operation Model*

#### 2.2.1. Distributed Energy Resources

Common forms of distributed energy resources consist of wind and photovoltaic power. The specific output modeling is as follows:

(1) Wind-generated electricity

The effective output scope of wind power generation is determined by the wind speed being between the cut-in and cut-out levels.

$$P_{WPP,t} = \begin{cases} 0, 0 \le v_t \le v_{in}, v_t > v_{out} \\ \frac{v_t^3 - v_{in}^3}{v_c^3 - v_{in}^3} g_c, v_{in} \le v_t \le v_c \\ g_c, v_c \le v_t \le v_{out} \end{cases} \quad (1)$$

where $P_{WPP,t}$ indicates the power of wind power generation at time $t$, which relies on $v_t$, the wind speed. $v_{in}$ and $v_{out}$ represent the cut-in and cut-out wind speeds of the fan, respectively. The rated power of wind power generation is denoted as $g_c$, which is achieved at the rated wind speed $v_c$.

(2) PV power generation

PV power generation primarily relies on solar radiation intensity, temperature and other factors received by the PV panel [19].

$$P_{PV,t} = S_{PV} \eta_{PV} r_t \quad (2)$$

where $P_{PV,t}$ indicates the power generated by the PV system at time $t$. $S_{PV}$ indicates the area of PV array. $\eta_{PV}$ represents the efficiency of the PV system in converting solar energy to electricity. $r_t$ indicates the direct solar irradiance at time $t$.

2.2.2. CHP Unit

The CHP unit consumes natural gas to provide users with stable power and heat energy, which is modeled as follows.

The CHP unit consumes natural gas to supply users with stable and dependable electricity and heat energy.

$$P_{CHP,t} = \alpha_g^e Q_{\text{gas},t}^{buy} H_g / 3600 \quad (3)$$

$$H_{CHP,t} = \eta_{eh} P_{CHP,t} \quad (4)$$

where $P_{CHP,t}$ and $H_{CHP,t}$ are the generation power and heating power of the CHP unit at time $t$, respectively. $Q_{buy,t}^{gas}$ indicates the volume of natural gas purchased by the MEG at time $t$. $\alpha_g^e$ indicates the power generation efficiency of CHP unit. $\eta_{eh}$ denotes the heat-to-electricity proportion for the CHP unit.

2.2.3. Energy Storage Device

The energy storage system offers small-scale electrical energy storage and helps stabilize the random fluctuations in renewable energy output due to its fast response capability.

$$E_{bat,t} = (1 - \chi_{bat}) E_{bat,t-1} + \alpha_{bat}^{ch} P_{bat,t}^{ch} \Delta t - \frac{P_{bat,t}^{dis} \Delta t}{\alpha_{bat}^{dis}} \quad (5)$$

where $E_{bat,t}$ denotes the electrical energy held within the storage unit at time $t$. $\chi_{bat}$ denotes the natural loss coefficient of the electric energy stored in the storage device. $P_{bat,t}^{ch}$ and $P_{bat,t}^{dis}$ are the charging and discharging power of the storage device at time $t$, respectively. $\alpha_{bat}^{ch}$ and $\alpha_{bat}^{dis}$ are the charge and discharge efficiency of the storage device, respectively.

### *2.3. Flexibility Response Mode*

Individual MEGs exhibit limited response capacity due to their constrained capacity and spatial coverage. However, collaborative response from geographically proximal MEG

clusters can deliver substantial flexibility response capacity to host utility grid dispatching demands. This cluster-based coordination mechanism demonstrates enhanced grid support potential compared to standalone operation. The optimized operational architecture for MEG cluster flexibility response to host utility grid coordination is illustrated in Figure 2.

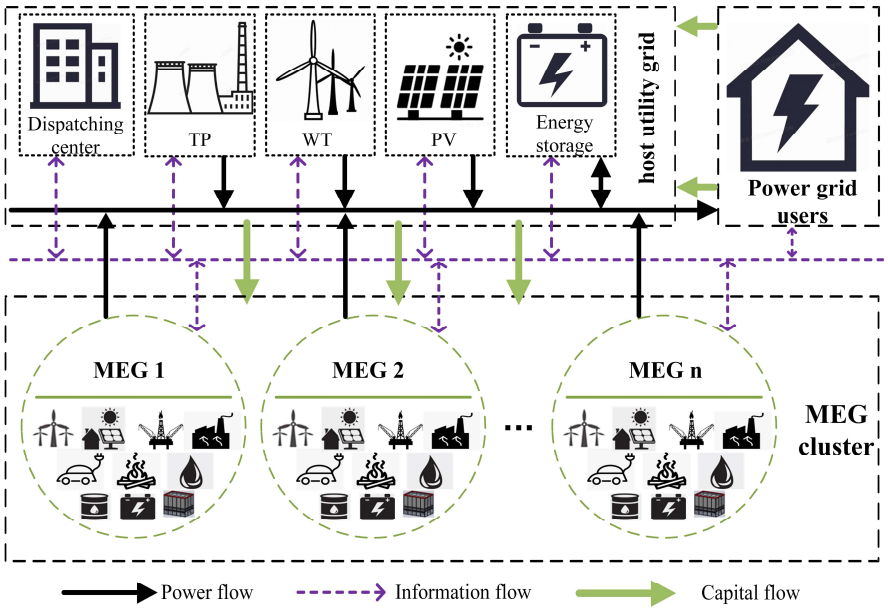



**Figure 2.** MEG response to host utility grid operation structure.

As depicted in Figure 2, individual MEGs first calculate their available power capacity and generation costs based on optimal self-dispatch plans while maintaining internal supply/demand balance. These parameters, including power availability limits and bidding information, are subsequently transmitted to the higher-level power grid. The host utility grid then determines each MEG's actual dispatchable power by evaluating aggregated response capacities and cost bids across the MEG cluster, followed by issuing dispatch commands to individual MEGs. Finally, the host utility grid settles revenues for the MEG cluster according to the actual dispatched power. The procedural workflow for MEG cluster response to host utility grid coordination is illustrated in Figure 3.

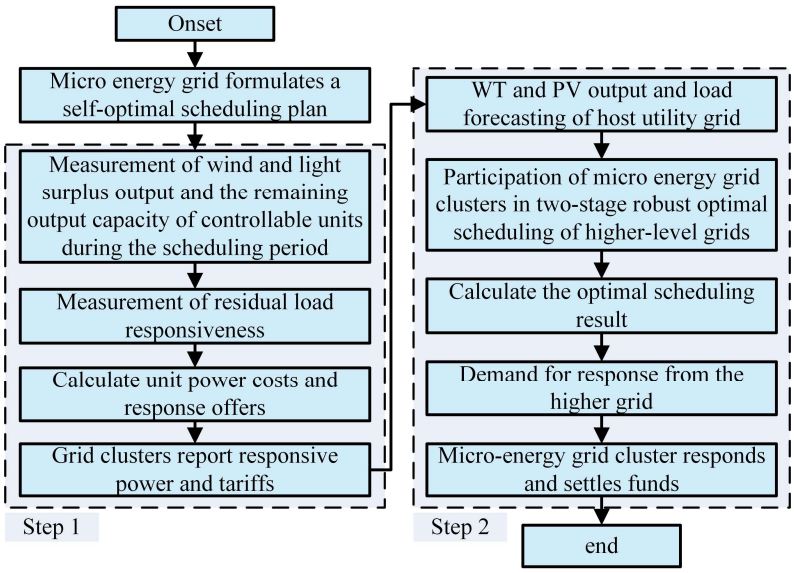



**Figure 3.** Steps for MEG clusters to respond to the host utility grid.

## 3. Measurement Model of Flexible Response Capability of MEG Clusters

### *3.1. MEG Scheduling Optimization Model*

#### 3.1.1. Objective Function

The operation of MEGs needs to achieve the minimum operating cost under the premise of meeting the load demand. The operating cost includes fuel cost, equipment maintenance cost, and power abandonment penalty cost.

$$\begin{cases} F_1 = \sum_{t=1}^{T} (C_{commute,t} + C_{om,t} + C_{abandon,t}) \\ C_{commute,t} = \left\{ \xi_{heat,t} \left( H_{buy,t} - H_{sell,t} \right) + \xi_{gas,t} Q_{buy,t}^{gas} \right\} \Delta t \\ C_{om,t} = \sum_{i \in \Omega_{all}} \sum_{s \in \Omega_s} \left\{ K_{om,i} P_{i,t} + K_{om,s} \left[ u_{bat,t} P_{bat,t}^{ch} + (1 - u_{bat,t}) P_{bat,t}^{dis} \right] \right\} \Delta t \\ C_{abandon,t} = \xi_{abandon} P_{abandon,t} \Delta t \end{cases} \tag{6}$$

where $F_1$ indicates the total operating cost of MEG. $C_{commute,t}$, $C_{om,t}$, and $C_{abandon,t}$ correspond to expenses on fuel, costs of operation and maintenance, and penalty costs from renewable energy abandonment, respectively. $H_{buy,t}$ and $H_{sell,t}$ are purchase heat and sale heat of the MEG at time $t$. $P_{i,t}$ and $K_{om,i}$ are power and maintenance cost of equipment $i$. $K_{om,s}$ is the maintenance cost of energy storage equipment. $\xi_{heat,t}$, $\xi_{gas,t}$, and $\xi_{abandon}$ are heat price, gas price, and penalty cost respectively.

#### 3.1.2. Constraint Condition

The MEG operation process requires consideration of energy equilibrium limitations, generation facility restrictions, and energy storage unit limitations.

(1) Energy balance constraint

In MEG operation, constraints on electricity and heat energy supply/demand balance are important. The electricity supply/demand balance constraints are as follows:

$$\sum_i P_{i,t}^{power} (1 - \phi_i^{power}) + u_{bat,t} P_{bat,t}^{dis} = L_{power,t} + \sum_i P_{i,t}^{load} + (1 - u_{bat,t}) P_{bat,t}^{ch} \tag{7}$$

where $P_{i,t}^{power}$ and $\phi_i^{power}$ correspond to the power output and the internal power consumption rate of power generation equipment $i$. $P_{i,t}^{load}$ denotes controllable load $i$, and $L_{power,t}$ denotes user loads. $u_{bat,t}$ is the state of the battery, which is a 0–1 variable and the same below.

The constraints related to thermal energy balance are presented as follows:

$$L_{heat,t} + H_{sell,t} = H_{buy,t} + H_{CHP,t} \tag{8}$$

where $L_{heat,t}$ denotes heat load at time $t$.

(2) Equipment operation constraints

Within the MEG, all equipment must comply with operating power limits and also adhere to CHP unit ramping and start/stop constraints.

$$\begin{cases} P_{CHP}^{\min} \cdot U_{CHP,t} \le P_{CHP,t} \le P_{CHP}^{\max} \cdot U_{CHP,t} \\ -RD_{CHP}^{\max} \le P_{CHP,t} - P_{CHP,t-1} \le RU_{CHP}^{\max} \end{cases} \tag{9}$$

where $U_{CHP,t}$ serves as a 0–1 variable indicating the CHP unit's start/stop status. $RU_{CHP}^{\max}$ and $RD_{CHP}^{\max}$ stand for the upper and lower bounds of the ramping rate.

(3) Energy storage device constraints

The energy storage device must comply with the upper limit of input and output power and must not surpass its maximum capacity.

$$\begin{cases} (1-u_{bat,t})P_{bat}^{ch,\min} \le P_{bat,t}^{ch} \le (1-u_{bat,t})P_{bat}^{ch,\max} \\ u_{bat,t}P_{bat}^{dis,\min} \le P_{bat,t}^{dis} \le u_{bat,t}P_{bat}^{dis,\max} \\ E_{bat}^{\min} \le E_{bat,t} \le E_{bat}^{\max} \end{cases} \tag{10}$$

where the energy storage device has upper limits for charging and discharging power, which are denoted by $P_{bat}^{ch,\max}$ and $P_{bat}^{dis,\max}$. $E_{bat,t}$ denotes the capacity at time $t$.

### *3.2. Measurement of Flexibility Response Capability*

The prerequisite for realizing the flexibility response in MEG clusters lies in quantifying their flexibility response capacity and determining cost bids for providing such services. Therefore, based on the optimal self-dispatch plans derived from Section 3.1, we systematically assess surplus generation capacities across key components, including WT/PV generation, CHP units, and demand-responsive loads.

#### 3.2.1. Power Supply Side Surplus Power Generation Capacity

Under scenarios of abundant wind/PV generation, MEGs frequently encounter internal renewable energy curtailment due to insufficient local absorption capacity. Additionally, optimal self-dispatch plans rarely maintain full-load operation of generation units throughout the dispatch period. Therefore, we systematically evaluate surplus generation capacities from WT/PV systems, CHP units, and energy storage systems, outlined below.

$$P_{power,t}^{\prime n} = P_{RE,t}^{\prime n} + P_{CHP,t}^{\prime n} + P_{bat,t}^{\prime n} \tag{11}$$

where $P_{power,t}^{\prime n}$ quantifies the maximum permissible surplus generation capacity from the source-side infrastructure of MEG $n$ at time $t$. $P_{RE,t}^{\prime n}$, $P_{CHP,t}^{\prime n}$, and $P_{bat,t}^{\prime n}$ denote the peak residual generation thresholds for distributed renewable assets, cogeneration unit dispatchable reserves, and energy storage system regulation capacity within the MEG $n$.

Among them, the residual generation potential of WTs and PV installations is determined through the following computation:

$$P_{RE,t}^{\prime n} = (\hat{P}_{WPP,t} - P_{WPP,t}) + (\hat{P}_{PV,t} - P_{PV,t}) \tag{12}$$

where $\hat{P}_{WPP,t}$ and $\hat{P}_{PV,t}$ denote the forecasted wind and photovoltaic generation values. $P_{WPP,t}$ and $P_{PV,t}$ represent the planned output of wind power and PV power, respectively.

The calculation of residual output capacity of the CHP unit:

$$P_{CHP,t}^{\prime n} = P_{CHP}^{\max} - P_{CHP,t} \tag{13}$$

where $P_{CHP}^{\max}$ and $P_{CHP,t}$ correspond to the nameplate capacity and real-time generation setpoint of the CHP systems, respectively.

The real-time regulatory capacity of energy storage systems is governed by the synergistic interaction of rated discharge power and nominal storage capacity:

$$P_{bat,t}^{\prime n} = \min\left\{ \frac{E_{bat}^{\max} - E_{bat,t}}{\Delta t}, \left( P_{bat}^{dis,\max} - P_{bat,t}^{dis} \right) \right\} \tag{14}$$

3.2.2. Load-Side Depth-Response Capability

Within optimal self-dispatch plans, periods may exist where user demand response output remains below its maximum capacity. This underutilized DR potential represents deep demand response capacity, calculated as follows:

$$P_{load,\iota}^{In} = \phi_{DR} L_{power,\iota} - \Delta L_{PB,\iota} - \Delta L_{IB,\iota} \tag{15}$$

where $\Delta L_{PB,\iota}$ and $\Delta L_{IB,\iota}$ are price-based demand response (PBDR) and incentive demand response (IBDR) planned response at time $t$, respectively. $L_{power,\iota}$ denotes power demand at time $t$. $\phi_{DR}$ denotes the maximum threshold for load response.

The implementation of PBDR optimizes user consumption behaviors through time-variant pricing signals, shifting load cycles to thereby acquire deep response capacity. Both load shifting and curtailment may occur under PBDR schemes. The resultant load-side transferred or curtailed energy can be quantified via the price elasticity of demand.

$$\Delta L_{PB,t} = L_t^0 \times (e_{tt} \frac{\Delta P_t}{P_t^0} + \sum_{s=1\&s\neq t}^{24} e_{st} \frac{\Delta P_s}{P_s^0}) \tag{16}$$

$$e_{st} = \frac{\Delta L_s / L_s^0}{\Delta P_t / P_t^0} \tag{17}$$

where $\Delta L_{PB,t}$ represents the load response output of PBDR. $e_{tt}$ and $e_{st}$ denote the self-elasticity coefficient and cross-elasticity coefficient, respectively. The self-elastic effect exclusively induces load diminution, manifesting as a negative variation in demand. Conversely, the cross-elastic effect solely drives load redistribution between time intervals, characterized by a positive demand fluctuation.

Furthermore, MEGs implement IBDR to engage users in market regulation through incentive mechanisms, thereby acquiring load-side response capacity. The calculation formula for load variation under IBDR implementation is presented as follows:

$$\Delta L_{IB,t} = u_{IB,t}^{up} \Delta L_{IB,t}^{up} + u_{IB,t}^{dn} \Delta L_{IB,t}^{dn} \tag{18}$$

$$u_{IB,t}^{up} + u_{IB,t}^{dn} \leq 1 \tag{19}$$

where $\Delta L_{IB,t}$ represents the load response output of IBDR. $u_{IB,t}^{up}$ and $u_{IB,t}^{dn}$ are 0–1 variables, where 1 represents the implementation of load response and 0 represents the non-implementation of load response.

## 4. Optimization Model for MEG Cluster Flexibility Response to Host Utility Grid

### *4.1. Two-Stage Robust Theory*

Robust optimization constitutes a methodological framework for addressing system uncertainties [20]. While single-stage robust optimization tends to produce overly conservative solutions, two-stage robust optimization (alternatively termed adjustable robust or adaptive optimization) effectively addresses this limitation. Tailored to power dispatch characteristics, this section develops a generic two-stage robust optimization model, with its deterministic compact formulation represented in Equation (20).

$$\begin{cases} \min\limits_{x,y} c^T y \\ s.t. Dy \geq d \\ Ky = 0 \\ Fx + Gy \geq h \\ I_u y = \hat{u} \end{cases} \tag{20}$$

In this formulation, $x$ and $y$ denote optimization variables representing 0–1 state variables, and $y$ represents other decision variables. The objective function is weighted by coefficient vector $c$. $D$, $K$, $F$, $G$, and $I_u$ define the coefficient matrices associated with respective constraints. Constants $d$ and $h$ denote fixed column vectors. The inequality constraint $Dy \geq d$ enforces operational boundaries, whereas the equality constraint $Ky = 0$ imposes equilibrium conditions. The deterministic framework fixes $I_u y = \hat{u}$, ensuring PV output and load power align with their forecasted values across all time intervals. Here, colons denote specific relationships between variables and constraints.

$$\hat{u} = [\hat{P}_{WPP,t}, \hat{P}_{PV,t}, \hat{L}_{power,t}]^T, t = 1, 2, \ldots, N_T \tag{21}$$

In this formulation, $\hat{L}_{power,t}$ represents predicted value of the load.

The proposed framework is computationally tractable through classical deterministic solvers, as it is formulated as a mixed-integer linear programming problem with inherent convexity properties. However, the optimality of dispatch solutions derived from this approach critically depends on forecasting accuracy, which cannot be guaranteed in practical MEG operations due to inherent stochastic disturbances. Consequently, deterministic optimization-based scheduling schemes often fail to meet real-world dispatch requirements, necessitating explicit incorporation of uncertainty impacts in modeling.

The stochastic deviations of WT and PV output and load demand are constrained within a bounded hyperrectangular uncertainty domain $U$, mathematically characterized as:

$$U = \begin{cases} u = [P_{WPP,t}, P_{PV,t}, L_{power,t}]^T \in R^{(N_T)\times 2}, t = 1, 2, \ldots, N_T \\ P_{WPP,t} \in [\hat{P}_{WPP,t} - \widehat{P}_{WPP,t}, \hat{P}_{WPP,t} + \widehat{P}_{WPP,t}] \\ P_{PV,t} \in [\hat{P}_{PV,t} - \widehat{P}_{PV,t}, \hat{P}_{PV,t} + \widehat{P}_{PV,t}] \\ L_{power,t} \in [\hat{L}_{power,t} - \widehat{L}_{power,t}, \hat{L}_{power,t} + \widehat{L}_{power,t}] \end{cases} \tag{22}$$

where $P_{WPP,t}$, $P_{PV,t}$, and $L_{power,t}$ are wind power, photovoltaic output power, and load power considering uncertainty. $\widehat{P}_{WPP,t}$, $\widehat{P}_{PV,t}$, and $\widehat{L}_{power,t}$ correspond to the upper limits for fluctuation deviations in wind power, photovoltaic output, and load power, respectively.

The bi-level robustness-oriented framework developed herein is designed to determine a cost-minimizing operational dispatch strategy under adversarial realizations of the bounded uncertainty parameter $u \in U$. The mathematical formalization of this dual-phase decision-making architecture is rigorously defined as:

$$\begin{cases} \min\limits_{x} \max\limits_{u\in U} \min\limits_{y\in\Omega(x,u)} c^T y \\ s.t. \quad x = (x_1, x_2, \ldots, x_{2\times N_T}) \\ x_i \in \{0, 1\}, \forall i \in (1, 2, \ldots, 2 \times N_T) \end{cases} \tag{23}$$

The primal/dual optimization architecture comprises two hierarchical layers: the outer layer corresponds to the first-stage decision-making program with design variable $x$, while the inner layer constitutes a nested adversarial optimization subproblem with recourse variables $u$ and $y$. This bi-level formulation is mathematically congruent with the economic dispatch cost minimization objective in Equation (20). The constraint-admissible

solution space $\Omega(x, u)$, characterizing all operationally feasible configurations under fixed $(x, u)$ pairs, is formally defined by the following polyhedral set:

$$\Omega(x,u) = \begin{cases} y & \\ Dy \geq d, & \rightarrow \gamma \\ Ky = 0, & \rightarrow \lambda \\ Fx + Gy \geq h, & \rightarrow v \\ I_u y = \hat{u}, & \rightarrow \pi \end{cases} \tag{24}$$

The dual variables $\gamma$, $\lambda$, $v$, and $\pi$ are associated with individual constraint equations in the recourse-level optimization subproblem.

Under any fixed uncertainty instantiation $u \in U$, the stochastic formulation in Equation (24) degenerates into the deterministic convex programming framework of Equation (21). The adversarial maximization operator embedded within the subordinate optimization layer seeks to delineate the cost-extremizing uncertainty configuration that induces peak expenditure trajectories within the operational paradigm.

### *4.2. Flexibility Response Two-Stage Robust Scheduling Optimization Model*

#### 4.2.1. Deterministic Model

Based on the description of Section 4.1, the host utility grid scheduling optimization aims to formulate the optimal scheduling plan of each subject under deterministic conditions.

(1) Objective function

The host utility grid's dispatch optimization objective function aims at minimizing total operational costs. Given the negligible generation costs of wind and PV plants, their marginal costs are disregarded. The cost components include thermal plant generation costs, energy storage dispatch costs, MEG cluster output costs, carbon emission costs, and renewable curtailment penalty costs. Additionally, MEG clusters incorporate an expected profit coefficient to determine response electricity prices based on aggregated dispatch costs and total generation output. The economic dispatch expenditure paradigm for enhanced electricity network scheduling is mathematically formalized through the subsequent analytical representation:

$$\min C_{total} = C_{MEG} + C_{TG} + C_{ES} + C_{CB} + C_{RE} + C_{OM} \tag{25}$$

where $C_{total}$ represents aggregated cross-temporal operational cost for resource orchestration, $C_{MEG}$ represents MEG cluster demand/response coordination cost, $C_{TG}$ represents generation cost of thermal power (TP), $C_{ES}$ represents distributed electrochemical storage capacity cost, $C_{CB}$ represents the carbon emission cost, $C_{RE}$ represents variable renewable energy integrated power generation cost, and $C_{OM}$ represents lifecycle reliability maintenance levy for critical infrastructure.

$$\begin{cases} C_{MEG} = \sum_{t=1}^{T}\sum_{n=1}^{N} \xi_{MEG,t}^{n}(1+\beta_n)P_{MEG,t}^{n} \\ C_{TG} = \sum_{t=1}^{T}\sum_{i=1}^{I} \xi_{coal} u_{TG,t}^{i}(a_{coal}^{i}{P_{TG,t}^{i}}^{2} + b_{coal}^{i}P_{TG,t}^{i} + c_{coal}^{i}) \\ C_{ES} = \sum_{t=1}^{T} \xi_{ES,t}(u_{ES,t}^{out}P_{ES,t}^{out} - u_{ES,t}^{in}P_{ES,t}^{in}) \\ C_{CB} = \sum_{t=1}^{T}\sum_{n=1}^{N}\sum_{i=1}^{I} \xi_{carbon}(\sigma_{CO_2}^{i,TG}P_{TG,t}^{i} + \sigma_{CO_2}^{i,MEG}P_{MEG,t}^{i}) \\ C_{RE} = \sum_{t=1}^{T}\left\{K_{WPP}^{om}P_{WPP,t} + K_{PV}^{om}P_{PV,t} + \xi_{abandon}[(\hat{P}_{WPP,t} - P_{WPP,t}) + (\hat{P}_{PV,t} - P_{PV,t})]\right\} \\ C_{OM} = \sum_{t=1}^{T}\sum_{i=1}^{I}[K_{TG,i}^{om}P_{TG,t}^{i} + K_{ES}^{om}(u_{ES,t}^{out}P_{ES,t}^{out} + u_{ES,t}^{in}P_{ES,t}^{in}) \end{cases} \quad (26)$$

where $N$ denotes the MEG count within the MEG cluster. $P_{MEG,t}^{n}$ and $\beta_n$ correspond to the response power and expected return rate of MEG $n$. $\xi_{MEG,t}^{n}$ indicates the power generation cost of MEG $n$. $P_{WPP,t}$, $P_{PV,t}$, $P_{ES,t}^{in}$, and $P_{ES,t}^{out}$ represent the wind power, PV power, energy storage charge, and discharge power at time $t$. $\hat{P}_{WPP,t}$ and $\hat{P}_{PV,t}$ represent wind power and PV prediction power at time $t$, respectively. $P_{TG,t}^{i}$ denotes real-time active power output of the $i$th TP unit. $a_{coal}^{i}$, $b_{coal}^{i}$, and $c_{coal}^{i}$ represent the coal consumption coefficient of the TP unit. $\xi_{coal}$, $\xi_{carbon}$, $\xi_{abandon}$, and $\xi_{ES,t}$ represent the time-dependent fuel cost for TP generation, carbon pricing coefficient under emission cap constraints, penalty price for renewable energy curtailment, and time-of-use tariff for energy storage charging/discharging operations, respectively. $\sigma_{CO_2}^{i,TG}$ and $\sigma_{CO_2}^{i,MEG}$ denote $CO_2$ emission intensity coefficients for TP and MEG systems, respectively. $u_{TG,t}^{i}$ denotes binary commitment status of the $i$th TP unit. $u_{ES,t}^{in}$ and $u_{ES,t}^{out}$ represent binary control variables for storage charge/discharge states. $K_{WPP}^{om}$ and $K_{PV}^{om}$ represent capital expenditure and operational expenditure for wind power conversion. $K_{TG,i}^{om}$ and $K_{ES}^{om}$ denote unit-specific maintenance cost rates for $i$th TP units and storage systems.

(2) Constraint condition

The dispatch coordination of higher-level power grid infrastructure must adhere to electric energy balance constraints while ensuring all generation units operate within dynamic power output boundaries defined by their technical specifications. In addition, MEG cluster response constraints, TP generation unit ramping limitations, and energy storage constraints should also be considered.

(1) Electric energy balance constraint

The host utility grid participating in the response of the MEG cluster needs to meet the power balance constraint.

$$\sum_{n=1}^{N} P_{MEG,t}^{n} + (1-\phi_{TG}^{power})\sum_{i=1}^{I} u_{TG,t}^{i}P_{TG,t}^{i} + (1-\phi_{WPP}^{power})P_{WPP,t} + (1-\phi_{PV}^{power})P_{PV,t} + u_{ES,t}^{out}P_{ES,t}^{out} = L_{grid,t} + u_{ES,t}^{in}P_{ES,t}^{in} \quad (27)$$

where $L_{grid,t}$ denotes the steady-state demand profile of the upper power grid. $\phi_{i}^{power}$ quantifies the loss coefficient characterizing auxiliary energy utilization within thermal generation facilities.

(2) MEG cluster constraints

The upper limit constraint and climbing constraint of residual output should be considered in the response of the MEG cluster to the host utility grid.

$$\begin{cases} P^{n}_{MEG,t} \le P'^{n}_{power,t} + P'^{n}_{load,t} \\ -RD^{n,\max}_{MEG} \le P^{n}_{MEG,t} - P^{n}_{MEG,t-1} \le RU^{n,\max}_{MEG} \end{cases} \tag{28}$$

where $RD^{n,\max}_{MEG}$ denotes maximum allowable power descent rate for MEG $n$. $RU^{n,\max}_{MEG}$ denotes the threshold of instantaneous power ascent capacity for MEG $n$ complying with dispatch protocols.

(3) Thermal power unit constraints

The dispatchable power outputs from thermal generation systems must adhere to climbing constraints and start/stop constraints.

$$\begin{cases} (T^{i,on}_{TG,t-1} - M^{i,on}_{TG})(u^{i}_{TG,t-1} - u^{i}_{TG,t}) \ge 0 \\ (T^{i,off}_{TG,t-1} - M^{i,off}_{TG})(u^{i}_{TG,t} - u^{i}_{TG,t-1}) \ge 0 \\ -RD^{i,\max}_{TG} \le P^{i}_{TG,t} - P^{i}_{TG,t-1} \le RU^{i,\max}_{TG} \end{cases} \tag{29}$$

where $T^{i,on}_{TG,t-1}$ and $T^{i,off}_{TG,t-1}$ indicate cumulative online duration and accumulated offline period of unit $i$ at time $t-1$, respectively. $M^{i,on}_{TG}$ and $M^{i,off}_{TG}$ indicate the minimum technical operating duration and mandatory cooling interval of unit $i$, respectively.

(4) Energy storage constraints

The operational boundaries of electrochemical energy storage systems are governed by two fundamental dynamic constraints: power flux limitations and energy reservoir capacity.

$$\begin{cases} u^{in}_{ES,t} P^{in,\min}_{ES,t} \le P^{in}_{ES,t} \le u^{in}_{ES,t} P^{in,\max}_{ES,t} \\ u^{out}_{ES,t} P^{out,\min}_{ES,t} \le P^{out}_{ES,t} \le u^{out}_{ES,t} P^{out,\max}_{ES,t} \\ \varepsilon^{\min}_{ES} E^{\min}_{ES} \le E_{ES,t} \le \varepsilon^{\max}_{ES} E^{rate}_{ES} \\ u^{in}_{ES,t} + u^{out}_{ES,t} \le 1 \end{cases} \tag{30}$$

$$E_{ES,t} = (1 - \varepsilon_{ES}) E_{ES,t-1} + (\eta_{in} P^{in}_{ES,t} - \frac{1}{\eta_{out}} P^{out}_{ES,t}) \Delta t \tag{31}$$

The operational parameters governing energy storage systems are defined as follows: $P^{in,\min}_{ES,t}$ and $P^{in,\max}_{ES,t}$ denote the peak and valley thresholds for charging operations, $P^{out,\min}_{ES,t}$ and $P^{out,\max}_{ES,t}$ specify the permissible range for discharging processes, and $E_{ES,t}$ $E^{rate}_{ES}$ indicate real-time energy reserves and nominal storage capability. $\varepsilon_{ES}$, $\eta_{in}$, and $\eta_{out}$ indicate the self-loss coefficient and charge/discharge efficiency, respectively. $\varepsilon^{\min}_{ES}$ and $\varepsilon^{\max}_{ES}$ denote the operational boundaries of the power conversion system loading ratio.

4.2.2. Two-Stage Robust Reconstruction

During the stochastic optimization phase, considering uncertainties in wind and PV generation outputs, a box-type uncertainty set $U$ incorporating wind and photovoltaic generation is formulated on the basis of the uncertainty handling methods presented in Section 4.1.

$$U = \begin{cases} u = [P_{WPP,t}, P_{PV,t}]^{T}, t = 1, 2, \ldots, T \\ P_{WPP,t} \in [\hat{P}_{WPP,t} - \widehat{P}_{WPP,t}, \hat{P}_{WPP,t} + \widehat{P}_{WPP,t}] \\ P_{PV,t} \in [\hat{P}_{PV,t} - \widehat{P}_{PV,t}, \hat{P}_{PV,t} + \widehat{P}_{PV,t}] \end{cases} \tag{32}$$

where $\widehat{P}_{WPP,t}$ and $\widehat{P}_{WPP,t}$ denote the maximum fluctuation of wind power and photovoltaic power, respectively, both of which are positive. The fluctuation range is based on the predicted value and fluctuates up and down in the given deviation interval, which can be determined according to the previous prediction deviation.

Building upon this framework, the deterministic model for host utility grid dispatch optimization is reconstructed into a two-stage robust formulation that explicitly incorporates worst-case scenarios of the uncertainty variable $u$, thereby enabling the development of optimal dispatch strategies for host utility grids under extreme operational conditions.

$$\begin{cases} \min\limits_{x}(\max\limits_{u\in U}\min\limits_{y\in\Omega(x,u)} c^T y) \\ s.t. Dy \geq d \\ Ky = 0 \\ Fx + Gy \geq h \\ I_u y = u \end{cases} \tag{33}$$

The optimization model features a two-layer structure: the upper-level optimization framework defines the initial decision-making phase through strategic variable $x$, whereas the nested max-min formulation encapsulates the subsequent adaptive phase for uncertainty resolution within the bi-level architecture. This nested formulation aims to identify worst-case operational scenarios and determine optimal solutions under these identified scenarios, with decision variables $u$ and $y$ governing uncertainty realization and adaptive responses, respectively.

Here, the specific expressions of $x$ and $y$ are specified as follows:

$$\begin{cases} x = [\underbrace{u^{in}_{ES,t}, u^{out}_{ES,t}}_{ES}, \underbrace{u^{1}_{TG,t}, \ldots, u^{i}_{TG,t}}_{TG}]^T \\ y = [\underbrace{P^{1}_{MEG,t}, \ldots, P^{n}_{MEG,t}}_{MEGs}, \underbrace{P^{1}_{TG,t}, \ldots, P^{i}_{TG,t}}_{TG}, \underbrace{P_{WPP,t}, P_{PV,t}}_{RE}, \underbrace{P^{in}_{ES,t}, P^{out}_{ES,t}}_{ES}]^T \end{cases} \tag{34}$$

In Equation (33), $c$ represents the coefficient matrix corresponding to Equations (25) and (26). $D$, $K$, $F$, $G$, and $I_u$ represent the constraint condition coefficient matrix corresponding to the objective function. $d$ and $h$ represent the corresponding constant column vector. $Dy \geq d$ represents inequality constraints, corresponding to Equations (28) and (30). $Ky = 0$ represents the equality constraint, corresponding to Equations (27) and (31). $Fx + Gy \geq h$ corresponds to Equation (29). The equality constraint $I_u y = u$ characterizes the forecasted generation profiles for wind and photovoltaic resources. The domain $\Omega(x, u)$ delineates the admissible solution space for the decision variable $y$, which dynamically evolves in response to uncertainty parameter variations within prescribed bounds. Under predefined parametric configurations of $(x, u)$, the bi-level adaptive robust scheduling framework reduces to its deterministic counterpart, formally expressed as:

$$\Omega(x,u) = \begin{cases} y & \\ Dy \geq d, & \to \gamma \\ Ky = 0, & \to \lambda \\ Fx + Gy \geq h, & \to v \\ I_u y = \hat{u}, & \to \pi \end{cases} \tag{35}$$

where $\gamma$, $\lambda$, $v$, and $\pi$ stand for the dual variables associated with each constraint row in the second-stage minimization problem.

To solve this bi-level problem, we implement the Column-and-Constraint Generation (C&CG) algorithm [21], which decomposes the problem into a master problem (first-stage decisions) and a subproblem (worst-case uncertainty identification).

## 5. Example Analysis

### *5.1. Basic Data*

This section conducts case studies using a southern China-based MEG as the benchmark system. The MEG configuration comprises 280 kW of wind power, 220 kW of PV generation, 60 kW of distributed energy storage, and two CHP units each rated at 70 kW. To simulate realistic grid-scale dispatch requirements, optimization results from four operational configurations of this MEG are utilized as empirical data for four distinct MEGs in numerical simulations. Subsequently, we quantify the flexibility response capacities of these four MEGs and scale their dispatchable power limits by a factor of 10 to emulate cluster-level response capabilities. Table 1 details the component configurations of each MEG, where checkmarks "√" denote the presence of specific units within individual MEGs.

**Table 1.** Configuration of MEG within the MEG cluster.

| Unit | MEG 1 | MEG 2 | MEG 3 | MEG 4 |
|---|---|---|---|---|
| WT | √ | - | √ | √ |
| PV | √ | √ | √ | √ |
| CHP | √ | √ | √ | - |
| Accumulator | √ | √ | - | √ |

The number and parameters of the configuration units of the above, MEG 1–4 are the same, and the conventional units such as TP, WT, PV, and energy storage are integrated into the dispatch coordination framework of transmission-level power networks. The system configuration comprises thermal power plants with 100 MW nameplate capacity, photovoltaic installations rated at 20 MW, and wind farms delivering 25 MW of nominal power output, and the TP unit includes a 20 MW unit, 30 MW unit, and 50 MW unit. The configuration parameters of the TP units and energy storage devices are presented in Table 2.

**Table 2.** Configuration parameters of each TP unit.

| TP Parameters | Unit 1 | Unit 2 | Unit 3 | Energy Storage Parameters | Electric Energy Storage |
|---|---|---|---|---|---|
| $P_{TG,t}^{i,\max}$(MW) | 20 | 30 | 50 | $E_{ES}^{\max}$(MWh) | 20 |
| $\sigma_{CO_2}^{i,TG}$(t/MWh) | 0.79 | 0.75 | 0.72 | $P_{ES,t}^{out\max}$(MW) | 5 |
| $a_{coal}^{i}\left(\mathrm{t/MW^2}\right)$ | 0.001124 | 0.000131 | 0.000169 | $P_{ES,t}^{out\min}$(MW) | 5 |
| $b_{coal}^{i}$(t/MW) | 0.28730 | 0.23222 | 0.27601 | $\eta_{in}/\eta_{out}$ | 0.9/0.9 |
| $c_{coal}^{i}$(t) | 4.07362 | 16.00726 | 11.46196 | $K_{ES}^{om}$(yuan/MW) | 18 |
| $RU_{TG}^{i,\max}$(MW/h) | 10 | 15 | 25 | $\varepsilon_{ES}^{\max}$ | 0.9 |
| $-RD_{TG}^{i,\max}$(MW/h) | 8 | 12 | 20 | $\varepsilon_{ES}^{\min}$ | 0.1 |
| $K_{TG,i}^{om}$(yuan/MW) | 13 | 10 | 9 | $\varepsilon_{ES}$ | 0.013 |

The regional power grid's coal price is CNY 685/ton, with a carbon emission price $\xi_{carbon}$ of CNY 500/ton. The renewable energy abandonment penalty $\xi_{abandon}$ is CNY 0.6/kWh, and the MEG's initial expected return rate $\beta_n$ is 0.05. At the same time, the energy

storage power station's charging and discharging price $\xi_{ES,t}$ follows the intraday electricity price. WT and PV conversion costs are CNY 0.3/kWh and CNY 0.35/kWh, respectively. Figure 4 shows the time-of-use electricity price and typical-day WT output, PV output, and load.

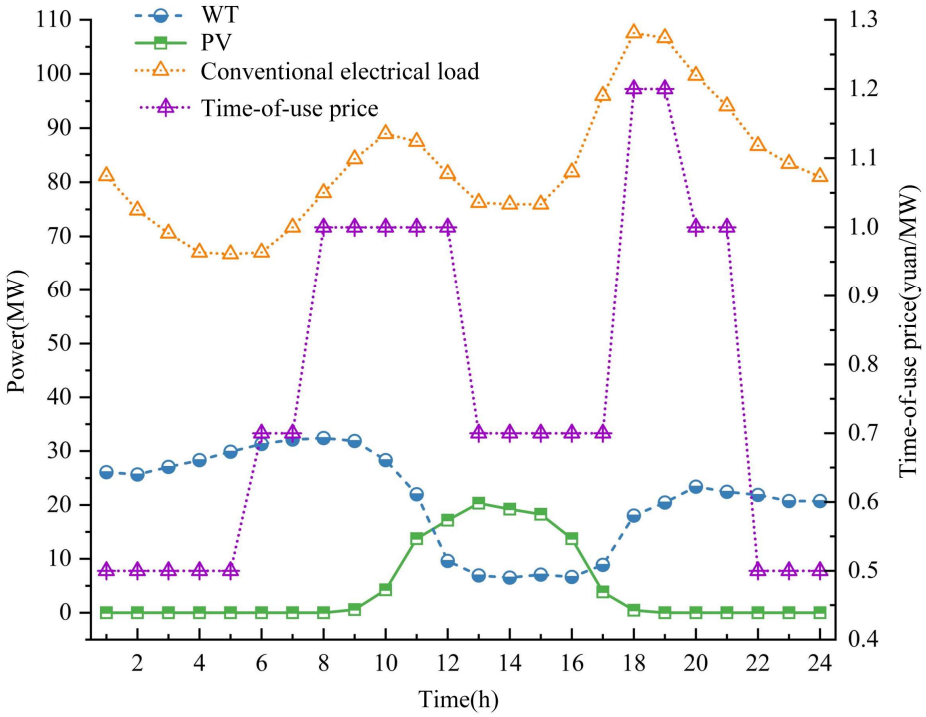



**Figure 4.** Typical daily load, wind and PV generation, and time-based electricity rates.

To investigate the impact of MEG participation on host utility grid dispatching, three comparative scenarios are constructed:

Scenario 1: MEGs pursue optimal self-dispatch plans without responding to grid dispatching requirements.

Scenario 2: Individual MEGs (MEG1–MEG4) separately respond to the host utility grid, analyzing single-MEG response effects.

Scenario 3: MEG clusters collectively respond through coordinated scheduling, identifying differential impacts between clustered and individual response modes.

### *5.2. Analysis of Effect*

The upper limit of the flexible response capability of the four MEGs is calculated, and the upper limit of the response output during different periods is derived, with results illustrated in Figure 5.

As shown in Figure 5, the dispatchable power capacity limits of MEG1–MEG3 peak during the 09:00–11:00 period and reach minimum values at 20:00–21:00. MEG4 exhibits substantially lower total capacity limits, equivalent to only 49.1%, 53.3%, and 57.1% of MEG1–MEG3, respectively. This discrepancy stems from divergent internal component configurations among the MEGs, which directly determine their dispatchable power potential. The optimal dispatch scheme for MEGs without grid response participation is presented in Figure 6.

In Scenario 1, the output of TP units peaks during the 17:00–20:00 period due to concurrent user electricity demand peaks and renewable generation decline, necessitating increased thermal output to maintain supply/demand balance. Notably, this thermal output surge coincides with MEG response trough periods. By incorporating MEG flexibility

response capacity limits as constraints, the optimal dispatch schemes for Scenarios 2–3 are derived and illustrated in Figures 7 and 8.

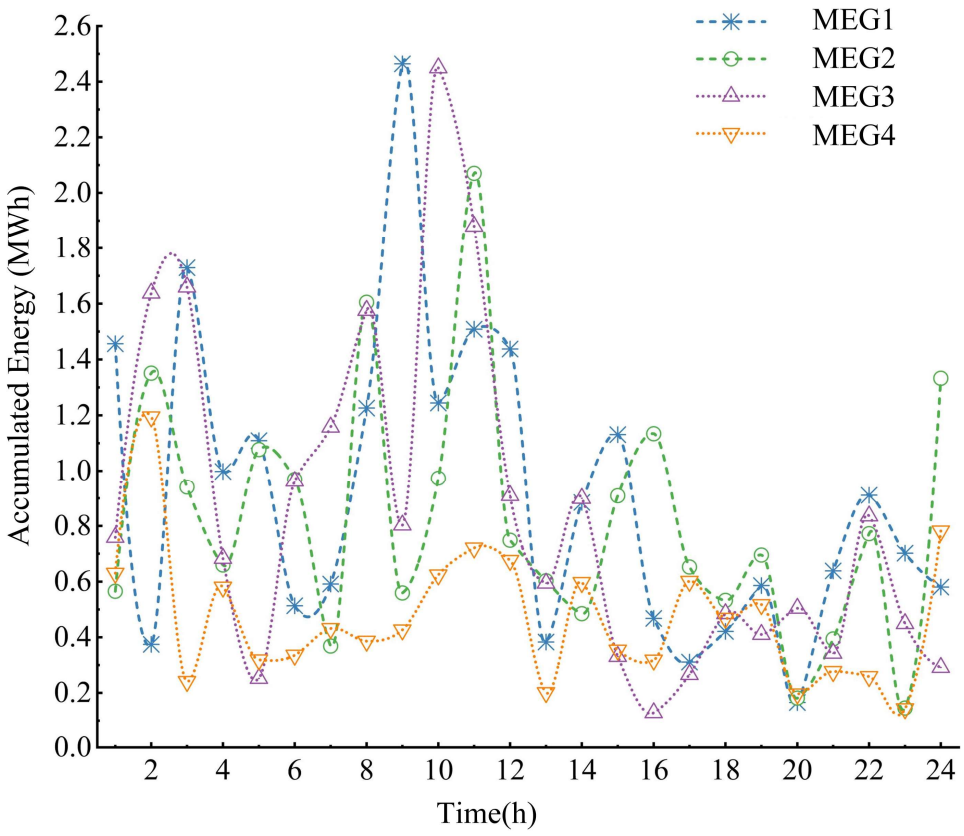



**Figure 5.** Results of MEG flexibility responsiveness measurements.

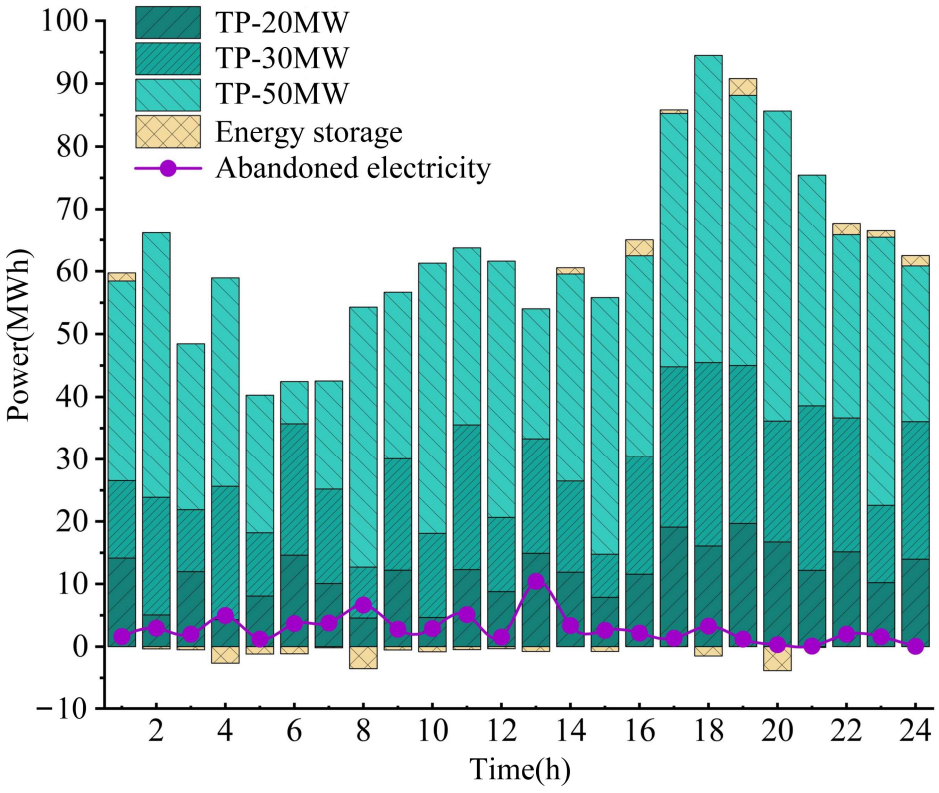
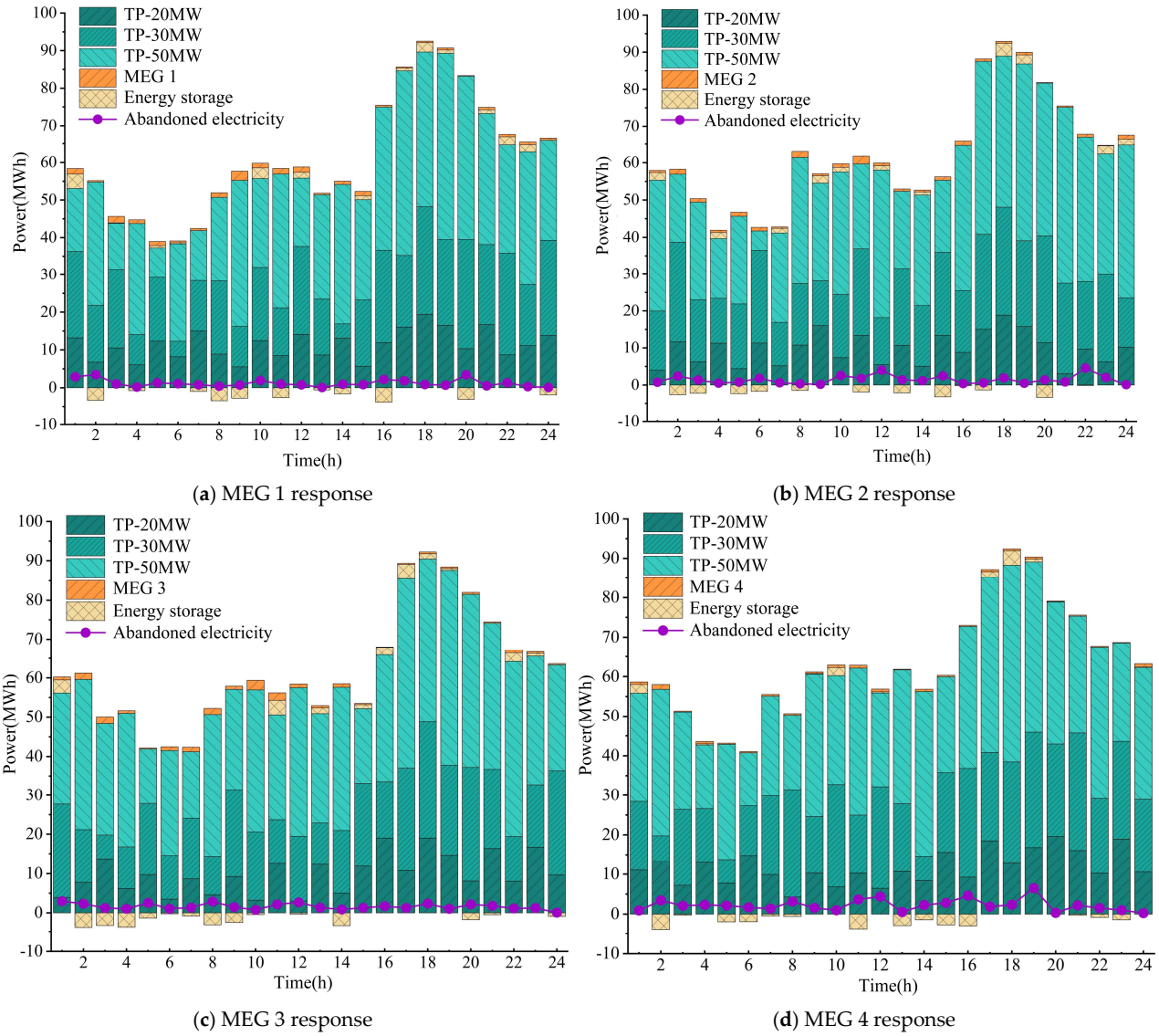


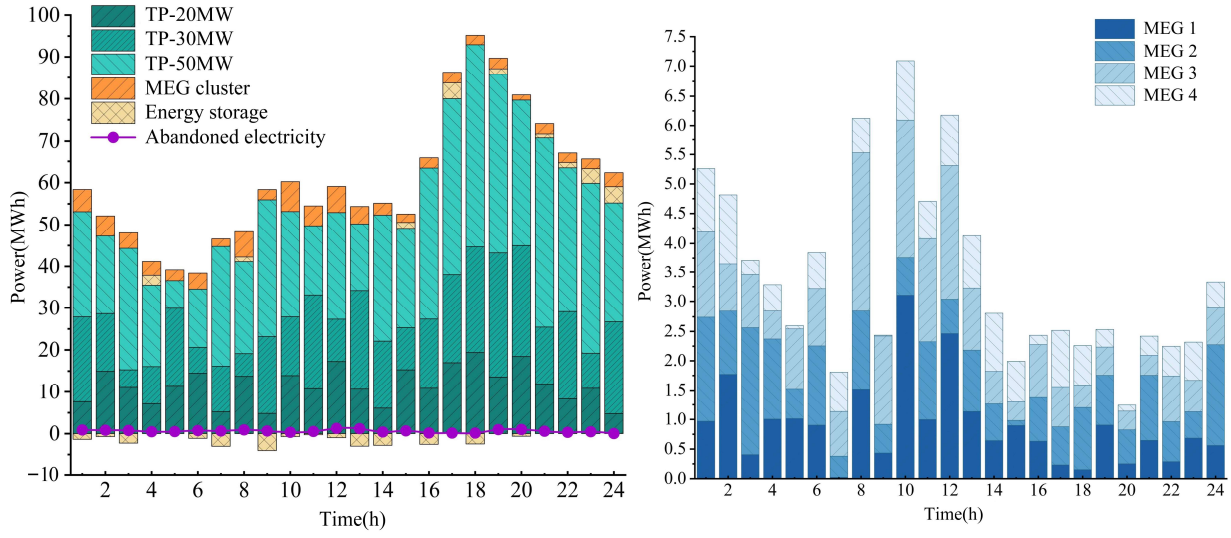

**Figure 6.** Scenario 1 optimal scheduling program.




(**a**) MEG 1 response (**b**) MEG 2 response

(**c**) MEG 3 response (**d**) MEG 4 response

**Figure 7.** Scenario 2 optimal scheduling program.




(**a**) Optimal scheduling scheme of cluster response power grid (**b**) MEG cluster output

**Figure 8.** Scenario 3 optimal scheduling program.

Compared to Scenario 1, Scenario 2 demonstrates significant reductions in TP unit peak/valley differences by 3.3%, 9.1%, 9.2%, and 10.8%, respectively. Concurrently, peak-hour thermal generation decreases by 5.1%, 5.9%, 4.3%, and 5.7%, indicating that MEG participation not only flattens thermal output profiles but also reduces ramping demands and peak regulation requirements. Figure 8 illustrates the optimal dispatch scheme under cluster response.

Scenario 3 achieves average TP reductions of 9.6%, 5.7%, 7.0%, 6.2%, and 9.7% compared to Scenario 1 and individual MEG responses, confirming enhanced smoothing of thermal output curves and further reductions in ramping costs and coal consumption. Paired *t*-tests confirm the significance of these reductions ($t = -4.32$, $p < 0.001$), with 95% confidence intervals for total cost spanning CNY $[129.45, 135.21] \times 10^4$. ANOVA further reveals significant differences in curtailment rates across scenarios ($F = 23.6$, $p < 0.001$), showing Scenario 3's superiority. The actual dispatched power of MEG1–MEG4 in Scenario 3 reaches 43.6%, 49.2%, 55.9%, and 57.6% of their capacity limits, reflecting cost-driven dispatch preferences: MEG4 exhibits the lowest response costs, while MEG1 incurs the highest. Table 3 summarizes comparative dispatch optimization results.

**Table 3.** Optimization results of each unit scheduling in two scenarios.

| Numerical Value | | Scenario 1 | Scenario 2 | | | | Scenario 3 |
|---|---|---|---|---|---|---|---|
| | | | MEG 1 | MEG 2 | MEG 3 | MEG 4 | |
| **Total Costs ($10^4$ CNY)** | | **141.79** | **136.04** | **137.73** | **137.08** | **140.39** | **132.33** |
| Power (MW) | WT | 457.71 | | | | | |
| | PV | 100.50 | | | | | |
| | TP-20MW | 280.07 | 273.78 | 235.57 | 237.78 | 282.83 | 279.69 |
| | TP-30MW | 424.30 | 438.26 | 471.47 | 419.91 | 465.64 | 385.71 |
| | TP-50MW | 803.44 | 719.21 | 751.99 | 793.63 | 751.37 | 686.46 |
| | MEG 1 | - | 21.83 | - | - | - | 21.66 |
| | MEG 2 | - | - | 19.72 | - | - | 22.52 |
| | MEG 3 | - | - | - | 20.27 | - | 23.86 |
| | MEG 4 | - | - | - | - | 11.28 | 14.03 |
| | Energy storage charging | 18.68 | 24.84 | 22.69 | 25.77 | 25.41 | 25.95 |
| | Energy storage discharging | 12.65 | 19.47 | 19.80 | 19.69 | 11.06 | 19.55 |
| | Abandoned electricity | 67.42 | 28.67 | 34.69 | 38.49 | 53.89 | 14.50 |
| Power discard rate (%) | | 12.08 | 5.14 | 6.21 | 6.89 | 9.65 | 2.60 |

As shown in Table 3, Scenario 2 reduces dispatch costs by 4.1%, 2.9%, 3.3%, and 1.0% for MEG1–MEG4 relative to Scenario 1, while Scenario 3 achieves a 6.7% system-wide cost reduction. These results validate the economic superiority of MEG-enabled dispatching, with cluster coordination outperforming individual responses.

MEG participation substantially reduces wind/PV curtailment rates. Scenario 2 decreases curtailment by 6.94%, 5.87%, 5.19%, and 2.43% compared to Scenario 1, while Scenario 3 achieves a 9.48% reduction. Temporal curtailment patterns across scenarios are detailed in Figure 9.

Figure 9 reveals peak curtailment at 13:00 in Scenario 1, accounting for 15.5% of total curtailment. This occurs due to the combined effects of reduced load demand and increased renewable generation, coupled with thermal units' ramping limitations. In contrast, Scenario 3 reduces 13:00 curtailment to 11.4% of Scenario 1 levels, leveraging the MEG clusters' operational flexibility to balance supply/demand mismatches. Meanwhile,

curtailed energy in Scenario 3 is significantly lower than in Scenario 1 (ANOVA: F = 23.6, $p < 0.001$; Tukey HSD: $p < 0.01$).

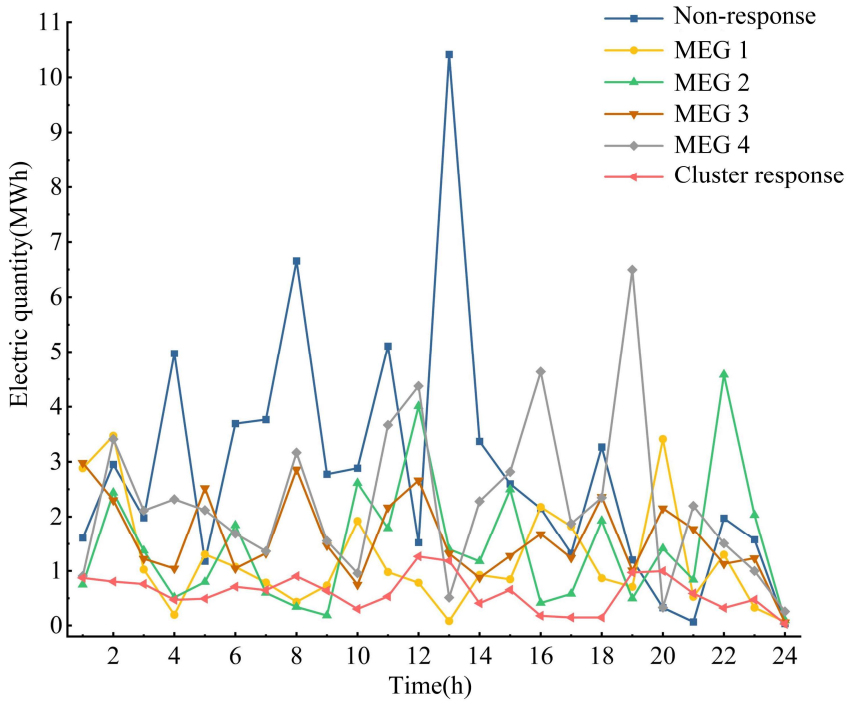



**Figure 9.** Wind and PV energy discarded in different scenarios.

Furthermore, maximum curtailment in Scenarios 2 and 3 drops to 33.3%, 44.0%, 28.6%, 62.4%, and 12.1% of Scenario 1 values, demonstrating that higher response capacities correlate with flatter curtailment profiles. Figure 10 compares MEG response patterns between scenarios.

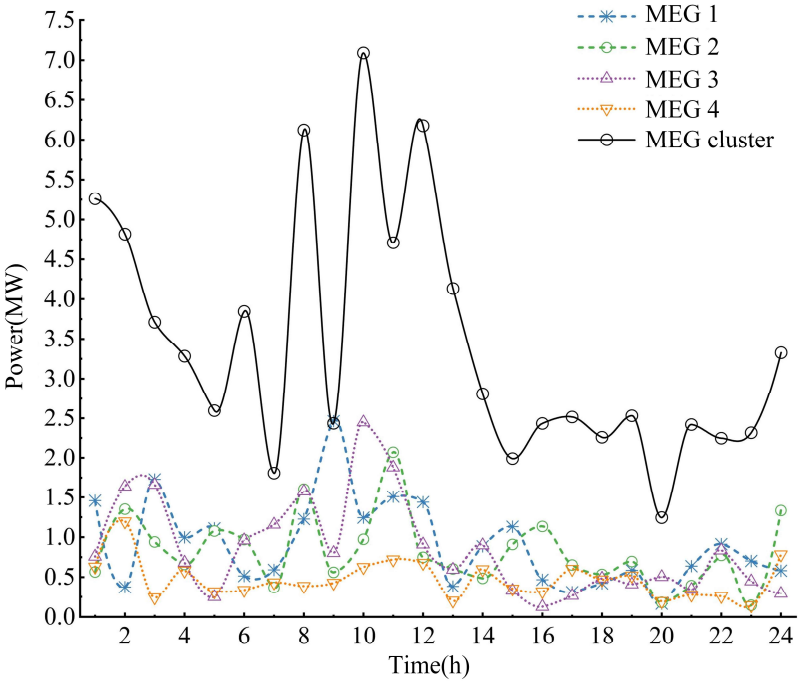



**Figure 10.** MEG response program.

Figure 10 highlights maximum response fluctuations during 09:00–10:00 under cluster and individual (MEG1/MEG4) responses, triggered by concurrent load increases and

renewable generation declines. Individual MEG1 and MEG4 ramping rates in this period reach only 57.4% and 21.1% of cluster-level ramping, respectively, underscoring the superior flexibility of coordinated MEG clusters in reducing thermal ramping costs and curtailment.

## 6. Conclusions

To address the constrained grid-support capacity of individual MEGs, this paper establishes the operation mode of the MEG clusters to respond flexibly to the host utility grid. Building upon the optimal self-scheduling plan of the MEG, its flexibility response capability is measured. Subsequently, a two-stage robust optimization model is constructed to manage renewable generation uncertainties in the process of interaction between the MEG cluster and host utility grid. Case study results demonstrate the following:

(1) MEG clusters effectively respond to host utility grid dispatching demands, reducing overall operational costs by 6.7% compared to autonomous grid optimization while outperforming individual MEG responses. The cluster-based approach demonstrates a positive correlation between dispatched response capacity and cost reduction magnitude. Concurrently, renewable curtailment rates decrease significantly, with cluster response achieving a 9.48% reduction in wind/PV curtailment, substantially improving system-wide economic efficiency.

(2) The proposed two-stage robust model effectively mitigates renewable generation uncertainties, reducing curtailment variability by 58% under $\pm$20% forecast errors compared to conventional stochastic methods. This enhances grid operational stability while maintaining adaptability to extreme supply/demand mismatches. Additionally, compared to TP units, MEG clusters exhibit superior operational flexibility in balancing grid supply/demand dynamics, which can effectively replace some TP generation and flexibly adjust the power supply and demand balance of the host utility grid.

(3) Compared with the response of individual MEGs, the cluster response can smooth the output curve, further reduce the climbing and coal consumption cost of TP units, and reduce the abandoned power of new energy. The framework contributes to regional carbon neutrality targets by reducing coal consumption by 9.7%. Furthermore, the energy-centric bidding mechanism aligns with China's latest electricity market reforms, which prioritize MEG clusters as critical assets for low-carbon power systems.

While validated in a case in southern China, the framework's scalability requires further testing in regions with higher renewable volatility (e.g., coastal or arid zones). Future research will explore hybrid optimization architectures integrating chance-constrained programming to balance robustness with probabilistic market risks. Extensions to multi-energy markets, such as hydrogen storage arbitrage and carbon credit trading, may further enhance economic/environmental synergies. Additionally, benchmarking against distributed model predictive control and AI-driven scheduling paradigms may broaden the framework's applicability across diverse grid topologies.

**Author Contributions:** Conceptualization, H.Z. and Z.T; methodology, P.L.; validation, O.Z.; formal analysis, O.Z.; data curation, X.Y.; writing—original manuscript preparation, O.Z. and X.Y.; writing—review and editing, P.L.; visualization, H.Z.; supervision, Z.T. All authors have read and agreed to the published version of the manuscript.

**Funding:** This research was funded by the State Grid Henan Electric Power Company, grant number 5217L0240005.

**Data Availability Statement:** The data presented in this study are available on request from the corresponding author. The data are not publicly available due to institutional restrictions.

**Conflicts of Interest:** Hongkai Zhang, Peng Li, and Xianyu Yue are employed by the Economics Research Institute of the State Grid Henan Electric Power Company. The remaining authors declare that the research was conducted in the absence of any commercial or financial relationships that could be construed as a potential conflict of interest. The funders had no role in the design of the study; in the collection, analyses, or interpretation of data; in the writing of the manuscript; or in the decision to publish the results.

## Nomenclature

| Abbreviations | |
|---|---|
| MEG | micro-energy grid |
| DERs | distributed energy resources |
| DR | demand response |
| CHP | combined heat and power |
| PV | photovoltaic |
| WT | wind turbines |
| TP | thermal power |
| PBDR | price-based demand response |
| IBDR | incentive demand response |
| C&CG | Column-and-Constraint Generation |
| **Sets** | |
| $t$ | index for time |
| $i$ | index for equipment |
| $n$ | index for MEG |
| **Scalars** | |
| $\eta_{PV}$ | efficiency of the PV system in converting solar energy to electricity |
| $\alpha_g^e$ | power generation efficiency of CHP unit |
| $\eta_{eh}$ | heat-to-electricity proportion for the CHP unit |
| $\chi_{bat}$ | natural loss coefficient of the electric energy stored in the storage device |
| $\alpha_{bat}^{ch}$, $\alpha_{bat}^{dis}$ | charge and discharge efficiency of the storage device |
| $e_{tt}$, $e_{st}$ | self-elasticity coefficient and cross-elasticity coefficient |
| $\sigma_{CO_2}^{i,TG}$, $\sigma_{CO_2}^{i,MEG}$ | $CO_2$ emission intensity coefficients for TP and MEG systems |
| $\phi_i^{power}$ | loss coefficient characterizing auxiliary energy utilization within thermal generation facilities |
| $\varepsilon_{ES}$ | self-loss coefficient |
| $\eta_{in}, \eta_{out}$ | charge-discharge efficiency |
| **Parameter** | |
| $v_t$ | wind speed |
| $v_{in}$, $v_{out}$ | cut-in and cut-out wind speeds of the fan |
| $v_c$ | rated wind speed |
| $g_c$ | rated power of wind power generation |
| $S_{PV}$ | area of PV array |
| $r_t$ | direct solar irradiance at time $t$ |
| $RU_{CHP}^{\max}$, $RD_{CHP}^{\max}$ | upper and lower bounds of the ramping rate |
| $\phi_{DR}$ | maximum threshold for load response |
| $\beta_n$ | expected return rate of MEG $n$ |
| $a_{coal}^i, b_{coal}^i, c_{coal}^i$ | coal consumption coefficient of the TP unit |
| $\xi_{coal}$ | time-dependent fuel cost for TP generation |
| $\xi_{carbon}$ | carbon pricing coefficient under emission cap constraints |
| $\xi_{abandon}$ | penalty price for renewable energy curtailment |
| $\xi_{ES,t}$ | time-of-use tariff for energy storage charging/discharging operations |
| $RD_{MEG}^{n,\max}$ | maximum allowable power descent rate for MEG $n$ |
| $RU_{MEG}^{n,\max}$ | threshold of instantaneous power ascent capacity for MEG $n$ complying with dispatch protocols |
| $P_{ES,t}^{in,\min}$, $P_{ES,t}^{in,\max}$ | peak and valley thresholds for charging operations |
| $P_{ES,t}^{out,\min}$, $P_{ES,t}^{out,\max}$ | permissible range for discharging processes |
| $E_{ES,t}$, $E_{ES}^{rate}$ | real-time energy reserves and nominal storage capability |
| $\varepsilon_{ES}^{\min}$, $\varepsilon_{ES}^{\max}$ | operational boundaries of power conversion system loading ratio |
| **Variables** | |
| $P_{WPP,t}$ | power of wind power generation at time $t$ |
| $P_{PV,t}$ | power generated by the PV system at time $t$ |
| $P_{CHP,t}$ | generation power of the CHP unit at time $t$ |
| $H_{CHP,t}$ | heating power of the CHP unit at time $t$ |
| $Q_{buy,t}^{gas}$ | volume of natural gas purchased by MEG at time $t$ |
| $M_{TG}^{i,on}$, $M_{TG}^{i,off}$ | minimum technical operating duration and mandatory cooling interval of unit $i$ |
| $E_{bat,t}$ | electrical energy held within the storage unit at time $t$ |
| $P_{bat,t}^{ch}$, $P_{bat,t}^{dis}$ | charging and discharging power of the storage device at time $t$ |
| $F_1$ | total operating cost of MEG |
| $C_{communte,t}$ | expenses on fuel |
| $C_{om,t}$ | costs of operation and maintenance |
| $C_{abandon,t}$ | penalty costs from renewable energy abandonment |
| $H_{buy,t}$, $H_{sell,t}$ | purchase heat and sale heat of MEG at time $t$ |
| $P_{i,t}$, $K_{om,i}$ | power and maintenance cost of equipment $i$ |
| $K_{om,s}$ | maintenance cost of energy storage equipment |
| $\xi_{heat,t}$ | heat price |
| $\xi_{gas,t}$ | gas price |
| $\xi_{abandon}$ | penalty cost |
| $P_{i,t}^{power}$, $\phi_i^{power}$ | power output and the internal power consumption rate of power generation equipment $i$ |
| $P_{i,t}^{load}$ | controllable load $i$ |
| $L_{power,t}$ | user loads |
| $u_{bat,t}$ | state of the battery |
| $L_{heat,t}$ | heat load at time $t$ |
| $U_{CHP,t}$ | CHP unit's start/stop status |
| $P_{bat}^{ch,\max}$, $P_{bat}^{dis,\max}$ | maximum charging and discharging power of energy storage equipment |
| $E_{bat,t}$ | capacity at time $t$ |
| $P_{\text{power},t}^{\prime n}$ | maximum permissible surplus generation capacity from the source-side infrastructure of MEG $n$ at time $t$ |
| $P_{RE,t}^{\prime n}$ | peak residual generation thresholds for distributed renewable assets within the MEG $n$ |
| $P_{CHP,t}^{\prime n}$ | cogeneration unit dispatchable reserves within the MEG $n$ |
| $P_{\text{bat},t}^{\prime n}$ | energy storage system regulation capacity within the MEG $n$ |
| $\hat{P}_{WPP,t}$, $\hat{P}_{PV,t}$ | forecasted WT and PV generation values |
| $P_{WPP,t}$, $P_{PV,t}$ | scheduled dispatch targets for WT and PV power |
| $P_{CHP}^{\max}$, $P_{CHP,t}$ | nameplate capacity and real-time generation setpoint of CHP systems |
| $\Delta L_{PB,t}$, $\Delta L_{IB,t}$ | PBDR and IBDR planned response at time $t$ |
| $L_{power,t}$ | power demand at time $t$ |
| $u_{IB,t}^{up}$, $u_{IB,t}^{dn}$ | IBDR Response Status |
| $\hat{L}_{power,t}$ | predicted value of the load |
| $P_{WPP,t}$ | wind power |
| $P_{PV,t}$ | photovoltaic output power |
| $L_{power,t}$ | load power |
| $\widehat{P}_{WPP,t}$ | upper limits for fluctuation deviations in wind power |
| $\widehat{P}_{PV,t}$ | upper limits for fluctuation deviations in photovoltaic output |
| $\widehat{L}_{power,t}$ | upper limits for fluctuation deviations in load power correspondingly |
| $C_{total}$ | aggregated cross-temporal operational cost for resource orchestration |
| $C_{MEG}$ | MEG cluster demand/response coordination cost |
| $C_{TG}$ | generation cost of TP |
| $C_{ES}$ | distributed electrochemical storage capacity cost |
| $C_{CB}$ | carbon emission cost |
| $C_{RE}$ | variable renewable energy integrated power generation cost |
| $C_{OM}$ | lifecycle reliability maintenance levy for critical infrastructure |
| $P_{MEG,t}^n$ | response power of MEG $n$ |
| $\xi_{MEG,t}^n$ | power generation cost of MEG $n$. |
| $P_{ES,t}^{in}$, $P_{ES,t}^{out}$ | energy storage charge and discharge power at time $t$ |
| $P_{TG,t}^i$ | real-time active power output of the $i$th TP unit |
| $u_{TG,t}^i$ | binary commitment status of the $i$th TP unit |
| $u_{ES,t}^{in}$, $u_{ES,t}^{out}$ | binary control variables for storage charge/discharge states |
| $K_{WPP}^{om}$, $K_{PV}^{om}$ | capital expenditure and operational expenditure for wind power conversion |
| $K_{TG,i}^{om}$, $K_{ES}^{om}$ | unit-specific maintenance cost rates for $i$th TP units and storage systems |
| $L_{grid,t}$ | steady-state demand profile of the upper power grid |
| $T_{TG,t-1}^{i,on}$, $T_{TG,t-1}^{i,off}$ | cumulative online duration and accumulated offline period of unit $i$ at time $t-1$ |

## References


1. Wang, Z.; Chen, L.; Li, X.; Mei, S.A. Nash Bargaining Model for Energy Sharing between Micro-Energy Grids and Energy Storage. *Energy* **2023**, *283*, 129065. [CrossRef]
2. Ju, L.; Lu, X.; Li, F.; Bai, X.; Li, G.; Nie, B.; Tan, Z. Two-Stage Optimal Dispatching Model and Benefit Allocation Strategy for Hydrogen Energy Storage System-Carbon Capture and Utilization System-Based Micro-Energy Grid. *Energy Convers. Manag.* **2024**, *313*, 118618. [CrossRef]
3. Li, J.; Li, Y.; Ma, L.; Li, Z.; Ma, K. Research on Modeling and Control Strategy of Lithium Battery Energy Storage System in New Energy Consumption. *Energy Rep.* **2023**, *9*, 182–189. [CrossRef]
4. Yi, T.; Li, Q.; Zhu, Y.; Shan, Z.; Ye, H.; Xu, C.; Dong, H. A Hierarchical Co-Optimal Planning Framework for Microgrid Considering Hydrogen Energy Storage and Demand-Side Flexibilities. *J. Energy Storage* **2024**, *84*, 110940. [CrossRef]
5. Xiao, G.; Liu, H.; Nabatalizadeh, J. Optimal Scheduling and Energy Management of a Multi-Energy Microgrid with Electric Vehicles Incorporating Decision Making Approach and Demand Response. *Sci. Rep.* **2025**, *15*, 5075. [CrossRef]
6. Wang, J.; Lyu, C.; Bai, Y.; Yang, K.; Song, Z.; Meng, J. Optimal Scheduling Strategy for Hybrid Energy Storage Systems of Battery and Flywheel Combined Multi-Stress Battery Degradation Model. *J. Energy Storage* **2024**, *99*, 113208. [CrossRef]
7. Wu, N.; Wang, Z.; Li, X.; Lei, L.; Qiao, Y.; Linghu, J.; Huang, J. Research on Real-Time Coordinated Optimization Scheduling Control Strategy with Supply-Side Flexibility in Multi-Microgrid Energy Systems. *Renew. Energy* **2025**, *238*, 121976. [CrossRef]
8. Datta, J.; Das, D. Energy Management of Multi-Microgrids with Renewables and Electric Vehicles Considering Price-Elasticity Based Demand Response: A Bi-Level Hybrid Optimization Approach. *Sustain. Cities Soc.* **2023**, *99*, 104908. [CrossRef]
9. Armghan, H.; Xu, Y.; Bai, X.; Ali, N.; Chang, X.; Xue, Y. A Tri-Level Control Framework for Carbon-Aware Multi-Energy Microgrid Cluster Considering Shared Hydrogen Energy Storage. *Appl. Energy* **2024**, *373*, 123962. [CrossRef]
10. Zheng, Q.; Yang, P.; Wu, Y.; Xu, Z.; Zhang, P. Optimal Dispatch and Control Strategy of Park Micro-Energy Grid in Electricity Market. *Sustainability* **2023**, *15*, 15100. [CrossRef]
11. Liu, X.; Lu, H.; Zhao, W.; Chen, Y.; Shao, S. Research on Optimal Scheduling and Source-Network-Load Correlation Matching of Integrated Energy System Considering Uncertainty. *Energy* **2025**, *321*, 135421. [CrossRef]
12. Zhang, J.; Liu, Z.; Liu, Y. A Scheduling Optimization Model for a Gas-Electricity Interconnected Virtual Power Plant Considering Green Certificates-Carbon Joint Trading and Source-Load Uncertainties. *Energy* **2025**, *315*, 134470. [CrossRef]
13. Fan, Y.; Liu, W.; Zhu, F.; Wang, S.; Yue, H.; Zeng, Y.; Xu, B.; Zhong, P.-A. Short-Term Stochastic Multi-Objective Optimization Scheduling of Wind-Solar-Hydro Hybrid System Considering Source-Load Uncertainties. *Appl. Energy* **2024**, *372*, 123781. [CrossRef]
14. Feng, J.; Ran, L.; Wang, Z.; Zhang, M. Optimal Energy Scheduling of Virtual Power Plant Integrating Electric Vehicles and Energy Storage Systems under Uncertainty. *Energy* **2024**, *309*, 132988. [CrossRef]
15. Wang, T.; Hua, H.; Shi, T.; Wang, R.; Sun, Y.; Naidoo, P. A Bi-Level Dispatch Optimization of Multi-Microgrid Considering Green Electricity Consumption Willingness under Renewable Portfolio Standard Policy. *Appl. Energy* **2024**, *356*, 122428. [CrossRef]
16. Jani, A.; Karimi, H.; Jadid, S. Hybrid Day-Ahead and Real-Time Energy Trading of Renewable-Based Multi-Microgrids: A Stochastic Cooperative Framework. *Sustain. Energy Grids Netw.* **2024**, *40*, 101516. [CrossRef]
17. Lv, Q.; Wang, L.; Li, Z.; Song, W.; Bu, F.; Wang, L. Robust Optimization for Integrated Production and Energy Scheduling in Low-Carbon Factories with Captive Power Plants under Decision-Dependent Uncertainty. *Appl. Energy* **2025**, *379*, 124827. [CrossRef]
18. Ju, L.; Liu, L.; Han, Y.; Yang, S.; Li, G.; Lu, X.; Liu, Y.; Qiao, H. Robust Multi-Objective Optimal Dispatching Model for a Novel Island Micro Energy Grid Incorporating Biomass Waste Energy Conversion System, Desalination and Power-to-Hydrogen Devices. *Appl. Energy* **2023**, *343*, 121176. [CrossRef]
19. Ju, L.; Lu, X.; Yang, S.; Li, G.; Fan, W.; Pan, Y.; Qiao, H. A Multi-Time Scale Dispatching Optimal Model for Rural Biomass Waste Energy Conversion System-Based Micro-Energy Grid Considering Multi-Energy Demand Response. *Appl. Energy* **2022**, *327*, 120155. [CrossRef]
20. Lu, G.; Bai, X.; Qi, X.; Zhang, F.; Yan, X.; Feng, J.; Ju, L. Data-Model Fusing Driven Robust Configuration Optimization Model and Decision-Making Method for Renewable Energy Generation Base Considering Electric-Hydrogen Conversion. *Renew. Energy* **2025**, *241*, 122320. [CrossRef]
21. Ju, L.; Lv, S.; Zhang, Z.; Li, G.; Gan, W.; Fang, J. Data-Driven Two-Stage Robust Optimization Dispatching Model and Benefit Allocation Strategy for a Novel Virtual Power Plant Considering Carbon-Green Certificate Equivalence Conversion Mechanism. *Appl. Energy* **2024**, *362*, 122974. [CrossRef]


**Disclaimer/Publisher's Note:** The statements, opinions and data contained in all publications are solely those of the individual author(s) and contributor(s) and not of MDPI and/or the editor(s). MDPI and/or the editor(s) disclaim responsibility for any injury to people or property resulting from any ideas, methods, instructions or products referred to in the content.